Equivalent: Jurnal Ilmiah Sosial Teknik
Volume 8, Issue 5, 2350-2363
e_ISSN: 2775-0833
https://jurnalequivalent.id/index.php/jequi/index
DOI: doi.org/10.59261/jequi.v8i5.485

Flexural Strength Response of Coconut Coir Fiber-Reinforced Epoxy Composites Across Titanium Dioxide Contents

Mahadir Sirman[1]* Politeknik Ilmu Pelayaran Makassar, Indonesia

Syahrizal[2] Politeknik Ilmu Pelayaran Makassar, Indonesia

Muhammad Arsyad Suyuti[3] Politeknik Negeri Ujung Pandang, Indonesia

***Corresponding author:**
Mahadir Sirman, Politeknik Ilmu Pelayaran Makassar,
Indonesia. ✉mahadir@pipmakassar.ac.id

Article Info:

Article history:
Received: September 22, 2026
Revised: October 22, 2026
Accepted: October 26, 2026
Available Online: November 06, 2026

***Keywords*:**
Coconut Coir;
Epoxy;
Flexural Strength;
Three-Point Bending;
Titanium Dioxide

This is an open access article under the CC BY-SA license.

Copyright © 2026 by Author. Published by Cerdika International Cyber Polytechnic

Abstract

Background: Flexural performance is a critical design property of coconut coir fiber-reinforced epoxy composites; however, evidence regarding TiO_2-filled systems across multiple filler contents remains limited.

Objective: This study examined the flexural strength response of composites containing 0, 1, 3, 5, and 7 wt.% TiO_2 to determine whether any filled formulation exhibited flexural strength recovery toward that of the unfilled control.

Methods: Composites were fabricated using an epoxy-to-hardener ratio of 60:40, a matrix-to-fiber ratio of 75:25, and untreated, randomly oriented coir fibers approximately 50 mm long, using the hand lay-up method. Flexural testing was conducted in accordance with ASTM D790-25, with three specimens tested per formulation. Scanning electron microscopy (SEM) was used to examine the fracture surfaces. One-way analysis of variance (ANOVA), Tukey's honestly significant difference (HSD) test, Levene's test, Welch's ANOVA, and the Kruskal–Wallis test were employed to evaluate the results and assess the sensitivity of the findings to the limited replication.

Results: The mean flexural strengths of the 0, 1, 3, 5, and 7 wt.% TiO_2 formulations were 31.61 ± 3.75, 22.59 ± 0.62, 28.78 ± 1.42, 28.05 ± 0.87, and 30.66 ± 4.34 MPa, respectively. One-way ANOVA indicated statistically significant differences among the formulations (image). Tukey's HSD test identified statistically significant differences between the 0 and 1 wt.% formulations and between the 1 and 7 wt.% formulations. No TiO_2-filled formulation exhibited a statistically significant increase in flexural strength relative to the unfilled control. Sensitivity analyses highlighted the uncertainty associated with the small sample size, while SEM observations revealed interfacial debonding, fiber pull-out, interfacial gaps, fibrillation, and voids.

Conclusion: The 7 wt.% TiO_2 formulation exhibited the closest numerical recovery in flexural strength toward the unfilled control and therefore represents a candidate for further investigation. These findings should be interpreted cautiously because of the limited replication, incomplete metadata, and qualitative nature of the SEM observations.

To cite this article: Sirman, M., Syahrizal & Suyuti, M., A.. (2026). Flexural strength response of coconut coir fiber-reinforced epoxy composites across titanium dioxide contents. *Glosains: Jurnal Sains Global Indonesia, 7*(5), 2350-2363. https://doi.org/10.59784/glosains.v7i5.1023

INTRODUCTION

Natural fiber-reinforced polymer composites have been developed to produce lightweight materials while utilizing biomass residues (Kamarudin et al., 2022; Sankaran et al., 2025; Skosana et al., 2025). Coconut coir fiber is widely available and has a fibrous structure that makes it

suitable for reinforcing thermoset matrices (Madueke et al., 2024; Nissar et al., 2025; Okpala et al., 2021). However, variations in fiber diameter, random orientation, hydrophilic characteristics, and nonuniform fiber–matrix adhesion can result in heterogeneous mechanical responses. Under three-point bending, the upper surface of a specimen is predominantly subjected to compressive stress, while the lower surface is predominantly subjected to tensile stress, with shear stresses developing through the specimen thickness (Kallel & Elleuch, 2025; Khokhlov et al., 2025; Song et al., 2021). Therefore, flexural strength reflects the combined effects of the matrix, fibers, fiber–matrix interface, and processing defects (Brailson Mansingh et al., 2023; Faria et al., 2020). For coconut-coir/epoxy composites, the flexural response is particularly sensitive to fiber–matrix adhesion, fiber orientation, voids, and local processing heterogeneity, all of which can influence crack initiation and propagation under bending loads (Deeban et al., 2026).

ASTM D790-25 specifies procedures for determining the flexural properties of plastics and fiber-reinforced plastic composites using three-point loading of a simply supported rectangular specimen (Balaji et al., 2025). The resulting values are influenced by specimen dimensions, span-to-thickness ratio, test speed, conditioning, and material behavior at the maximum load. For anisotropic composites, values calculated using homogeneous beam theory should be interpreted as apparent flexural properties, and comparisons should be restricted to equivalent test configurations (ASTM International, 2025). Because the source records do not preserve complete information on specimen geometry, support span, crosshead speed, conditioning history, and fixture details, this manuscript describes the testing as following the reported principles of ASTM D790-25 rather than claiming independently verified compliance with all requirements of the standard.

Titanium dioxide (TiO_2) can function as a micro- or nanoscale filler that modifies stress transfer and crack propagation within the matrix (Anbanandam et al., 2026). Well-dispersed particles may fill voids, increase the effective interfacial area, restrict matrix deformation, and deflect propagating cracks. Conversely, particle agglomeration, increased viscosity, or inadequate fiber wetting can reduce flexural strength. Studies of bamboo/epoxy composites have reported the highest flexural properties at a relatively low TiO_2 content of 2 wt.% (Prabhu et al., 2024). Similarly, a study of luffa/epoxy composites reported a peak in flexural performance at a nano-TiO_2 content of 2 wt.% (Krishna et al., 2025). Differences in materials and processing conditions necessitate determining the effective filler content for each composite system. Comparisons with bamboo- and luffa-based composites are not used to assume that the optimum filler content is transferable across systems. Fiber chemistry and treatment, TiO_2 particle size and phase, matrix formulation, fiber content, dispersion method, and curing history may all influence the flexural response (Foruzanmehr et al., 2015). Accordingly, the 0–7 wt.% range is treated as an exploratory formulation series for the coconut-coir/epoxy system rather than as a range that presupposes an optimum.

The source research report contains several mechanical and environmental characterizations. The present article focuses exclusively on the flexural strength data to ensure that the research objectives, methods, analysis, discussion, and conclusions address a single mechanical response. This article presents a focused secondary analysis of the flexural strength and fracture-surface data contained in the source research dataset. No new specimens were manufactured for this manuscript, and the analysis does not claim to reconstruct test conditions independently when the relevant information is absent from the source records.

The study aims to: (1) quantify changes in flexural strength associated with the addition of TiO_2 at concentrations ranging from 0 to 7 wt.%; (2) evaluate the statistical significance and magnitude of the treatment effect; (3) identify treatment-group pairs exhibiting statistically significant differences; (4) distinguish numerical recovery toward the control value from statistically significant improvement relative to the control; and (5) examine fracture-surface morphology using scanning electron microscopy (SEM) to support the interpretation of failure mechanisms. The contribution of this focused analysis lies in integrating raw flexural strength observations, effect-size estimates, sensitivity analyses, and qualitative SEM evidence while explicitly limiting inferences according to the documented metadata and replication structure.

METHOD

Experimental Design and Variables

The study used a single-factor laboratory experimental design. The treatment factor was TiO_2 content, with five levels: 0, 1, 3, 5, and 7 wt.%. The response variable was maximum flexural strength (MPa). Each treatment level was represented by three specimens, yielding 15 specimen-level test results. The 0 wt.% group served as the control. The source report did not clarify whether the three specimens per treatment level were obtained from a single panel or from independently manufactured panels. This information was necessary to distinguish technical replication from process replication. Accordingly, each specimen was treated as an analytical observation, while the unknown panel of origin prevented confirmation that the three observations at each treatment level represented independent process replicates. Inferential results were therefore interpreted conditionally on the available specimen-level dataset.

Ingredients and Formulations

Table 1

Composite formulation in each treatment group

TiO_2 (wt.%)	Resin: Hardener	Matrix : Fiber	Fiber length	Fiber condition/orientation
0	60 : 40	75 : 25	±50 mm	Dry natural, untreated, random
1	60 : 40	75 : 25	±50 mm	Dry natural, untreated, random
3	60 : 40	75 : 25	±50 mm	Dry natural, untreated, random
5	60 : 40	75 : 25	±50 mm	Dry natural, untreated, random
7	60 : 40	75 : 25	±50 mm	Dry natural, untreated, random

Source: actual formulation in the 2026 research report. The calculation basis of wt.% TiO_2 needs to be confirmed from the mixing sheet.

The primary materials consisted of epoxy resin, hardener, coconut coir fiber, and TiO_2. The fibers were used in their natural, dry condition without chemical treatment, cut to approximately 50 mm in length, and randomly oriented. The resin-to-hardener ratio was 60:40, while the matrix-to-fiber ratio was 75:25. The brand and type of the resin and hardener, the TiO_2 supplier and purity, particle size and size distribution, anatase-to-rutile phase composition, fiber moisture content, and mass basis for the TiO_2 content were not documented in the source records available for this manuscript. These parameters were neither estimated nor reconstructed. Their absence was retained as a reproducibility limitation and restricted the extent to which differences in flexural strength could be attributed solely to TiO_2 content.

Composite Panel Manufacturing

The documented manufacturing stages included material preparation, TiO_2 weighing according to the reported formulation, fiber preparation, incorporation of TiO_2 into the resin, combination of the resin, hardener, and fibers, molding by hand lay-up or casting, compaction, curing, panel removal, and specimen cutting. Documentation of the manufacturing and testing stages from the source research is presented in Figure 1.



Figure 1. Documentation of materials, weighing, panel printing, specimen manufacturing, and mechanical testing stages on source research.

The stirring speed and duration, use of sonication or dispersants, order of hardener addition, vacuum degassing, pot life, compaction pressure, curing temperature and duration, and post-curing conditions were not recorded. These factors can influence viscosity, fiber wetting, TiO_2 agglomeration, and void content. Consequently, differences among the TiO_2-content groups could not be attributed exclusively to TiO_2 content because undocumented variations in mixing, dispersion, compaction, and curing may also have contributed to the observed flexural responses.



Figure 2. Example of epoxy/coconut coir/TiO_2 composite panel after molding and curing process.

Specimen Preparation and Three-Point Loading Principle

Method traceability status. The source report stated that the test followed the three-point-loading principle of ASTM D790-25. However, the specimen geometry and dimensions, support span, span-to-thickness ratio, support and loading-nose radii, crosshead speed, applicable Procedure A or B, conditioning conditions, testing-machine model, load-cell capacity, and test-termination criteria were not recorded. Therefore, the present manuscript does not claim independently verified full compliance with ASTM D790-25. The reported flexural results were interpreted as values obtained using the documented three-point-bending procedure, with the missing test metadata explicitly acknowledged as a limitation.

ASTM D790-25 specifies a three-point-bending configuration in which a rectangular, beam-shaped specimen is simply supported at two points and loaded at the center of the span. In this configuration, the maximum bending stress occurs at the outer surface near the center of the span. The standard distinguishes flexural strength, stress at break, and stress at a specified strain. The appropriate reported value depends on the load–deflection response and the specimen's failure behavior (ASTM International, 2025).



Figure 3. Schematic of three-point bending: central load (P), support span (L), specimen width (b), specimen thickness (d), and center deflection (D). Labels in the source schematic correspond to these English terms.

For rectangular specimens at small deflections, the maximum flexural stress was calculated by $\sigma f = 3PL/(2bd^2)$, where P is the maximum load or load at a set point (N), L is the span length (mm), b is the specimen width (mm), and d is the specimen thickness (mm). The outer surface strain can be calculated with $\varepsilon f = 6Dd/L^2$, with D as the center deflection of the span. This article used the flexural-strength values already calculated in the source dataset. Since the original P, L, b, d, D and load–deflection records are unavailable, the calculation could not be independently repeated or verified in the present analysis; the statistical conclusions therefore depend on the traceability of those source-derived MPa values.

Mandatory Testing and Metadata Protocols

The reconstructed testing protocol based on the reported three-point-bending principle comprised identifying each specimen by treatment level and replicate, measuring specimen width and thickness, determining the support span, positioning the specimen consistently on two supports, aligning the loading nose with the center of the span, applying the load at a controlled rate, recording the load–deflection curve, and documenting the maximum flexural stress and failure mode. Three specimen-level values per treatment level were included in the analysis. Because the source records did not establish whether these steps had all been performed and documented as specified, the reconstructed protocol was not treated as evidence of verified procedural compliance. Unavailable details are listed in Table 2 as unresolved metadata and were not estimated. These details should be recovered from the original laboratory records, where available; otherwise, they remain explicit limitations affecting reproducibility.

Table 2

Completeness of the flexure test method metadata

Parameters	Status on the source	Actions before submission
Reference standards	ASTM D790-25 Principle	A/B verification of compliance, methods, and procedures
Number of replications	3 per rate	Describe the source of the panel and randomization
Specimen geometry	Not yet available	Fill length, width, thickness, tolerance, and orientation
~~Spotlight~~ Span length	Not yet available	L fill and L/d ratio
Support/loading nose	Not yet available	Specimen radius, alignment, and contact fills
Tools and load cells	Not yet available	Brand/model content, capacity, and verification
Test speed	Not yet available	Fill in the crosshead rate or strain rate
Conditioning	Not yet available	Fill temperature, humidity, and duration

Curve and failure	Not yet available	Attach load-deflection and failure classification

Statistical Analysis

Each treatment group was summarized using the mean, sample standard deviation (SD), coefficient of variation (CV), and percentage change relative to the control. Differences among TiO_2-content groups were evaluated primarily using one-way analysis of variance (ANOVA) at a significance level of $\alpha = 0.05$. Tukey's honestly significant difference (HSD) test was used for pairwise comparisons only when the omnibus ANOVA result was statistically significant, with a family-wise error rate of 5%. The magnitude of the treatment effect was assessed using eta-squared (η^2) and omega-squared (ω^2). Variance homogeneity was assessed using the median-based Levene test. Welch's ANOVA and the Kruskal–Wallis test were used as sensitivity analyses to examine the robustness of the inferences under unequal-variance and rank-based alternatives, respectively. Because each treatment level contained only three specimens, assumption diagnostics and rank-based tests had limited statistical power. Furthermore, the independence of specimens from separate manufacturing panels could not be verified. Accordingly, the results were interpreted in conjunction with the raw data distribution, confidence intervals, effect sizes, and sensitivity analyses. No single (p)-value was treated as definitive.

Characterization of Fault Surface Morphology

Fracture-surface morphology was examined using a scanning electron microscope (SEM) at Politeknik Negeri Ujung Pandang (PNUP) at an accelerating voltage of 5.00 kV, in secondary-electron (SE) mode, and at working distances ranging from 7.2 to 19.7 mm. One representative specimen from each TiO_2-content group was examined at 100× magnification to assess fiber condition, fiber–matrix interfacial characteristics, and matrix defects. Observations at 1,000× magnification were used to examine fiber cross-sectional features, while additional observations at 5,000× magnification were performed on specimens from the 7 wt.% group.

Feature sizes were estimated from the scale bars and were therefore considered approximate. The analysis was qualitative; energy-dispersive X-ray spectroscopy (EDS), backscattered-electron (BSE) imaging, and quantitative measurements of fiber pull-out lengths and void fractions were not performed. The SEM model, conductive coating procedure, and location or origin of the examined fracture surfaces must be verified against the laboratory records before submission. Only one representative specimen per TiO_2-content group was imaged; therefore, the micrographs documented representative qualitative features and were not assumed to characterize every replicate. No compositional assignment to TiO_2 was made in the absence of supporting EDS or BSE evidence.

RESULTS AND DISCUSSION

Results

Descriptive Statistics and Dose-Response Patterns

Table 3

Raw data and descriptive statistics of flexural strength (n = 3 per level)

TiO_2 (wt.%)	S1	S2	S3	Average (MPa)	SD (MPa)	CV (%)	Δ control (%)	Group Tukey
0	29,82	29,10	35,92	31,61	3,75	11,85	0,00	a
1	23,30	22,25	22,21	22,59	0,62	2,74	-28,55	b
3	29,67	29,53	27,15	28,78	1,42	4,92	-8,95	ab
5	27,23	27,96	28,97	28,05	0,87	3,11	-11,26	ab
7	25,76	32,20	34,01	30,66	4,34	14,14	-3,03	a

Note: SD = standard deviation; CV = coefficient of variation; Δ control (%) = percentage change relative to the 0 wt.% control. Tukey letters summarize pairwise results at α = 0.05; with n = 3 per group, estimates of variability and group separation should be interpreted cautiously.

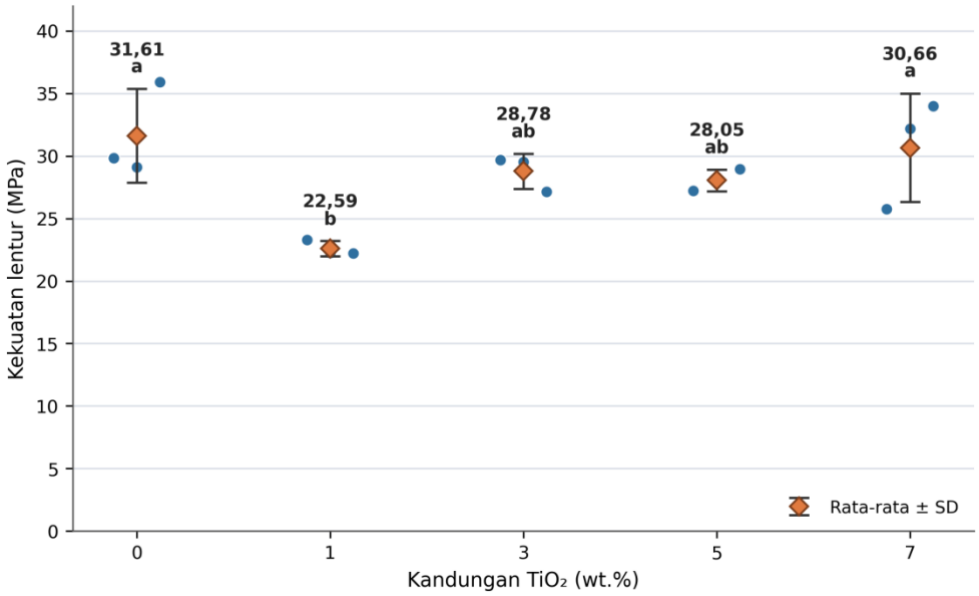


Figure 4. Individual data points, mean ± SD, and Tukey groups for flexural strength at each TiO_2 content.

The control yielded a flexural strength of 31.61 ± 3.75 MPa. The addition of 1 wt.% TiO_2 lowered the mean flexural strength to 22.59 ± 0.62 MPa, representing a 28.55% decrease relative to the control mean. The value increased to 28.78 ± 1.42 MPa at 3 wt.% and 28.05 ± 0.87 MPa at 5 wt.%. At 7 wt.%, the mean strength reached 30.66 ± 4.34 MPa, only 3.03% below the control mean. Thus, no TiO_2-filled formulation exceeded the control mean, and the 7 wt.% formulation showed the closest numerical recovery toward the control among the filled formulations, without demonstrating a statistically significant difference from the control. The nonlinear pattern may reflect a combination of particle dispersion, changes in resin viscosity, fiber distribution, interfacial adhesion, and void formation. However, these mechanisms remain hypotheses rather than directly measured causal pathways.

The 1 wt.% group had the lowest coefficient of variation (CV), at 2.74%, indicating low relative dispersion among the three specimen-level measurements for that formulation. However, this observation does not establish a mechanism for the reduction in flexural strength. In contrast, the 7 wt.% group had the highest CV, at 14.14%. One specimen had a flexural strength of 25.76 MPa, whereas the other two reached 32.20 and 34.01 MPa. This variation suggests that the mean strength at 7 wt.%, although close to the control mean, should be verified using an independent manufacturing panel. The higher CV at 7 wt.% is consistent with greater specimen-to-specimen heterogeneity and reinforces the need for independent panel replication before process-level conclusions can be drawn.

ANOVA, Effect Measurement, and Sensitivity Analysis

Table 4
One-way ANOVA of flexural strength

Source of variation	SS	df	MS	F	p
Between TiO_2 rates	148,384	4	37,096	5,153	0,016
In groups	71,987	10	7,199	–	–
Total	220,370	14	–	–	–

Note: SS = Sum of Squares; MS = Mean Square; $\eta^2 = 0.673$ and $\omega^2 = 0.526$ are effect-size estimates for the observed dataset.

One-way ANOVA indicated a statistically significant effect of TiO_2 content on flexural strength, $F(4, 10) = 5.153$, $p = 0.016$. The observed $\eta^2 = 0.673$ indicates that a large proportion of the sample variance was associated with between-group differences. However, this estimate

should not be generalized as a population-level percentage of explained variability. The bias-adjusted effect-size estimate, $\omega^2 = 0.526$, also indicated a large effect. The median-based Levene test found no evidence of variance heterogeneity, W = 0.708, p = 0.604; however, its interpretation is limited by the small sample size of three specimens per group. The large η^2 and ω^2 estimates should therefore be interpreted cautiously because of the small group sizes and the uncertainty surrounding the independence of the specimen replicates.

Welch's ANOVA also yielded a statistically significant result, F(4, 4.67) = 20.681, p = 0.003. In contrast, the Kruskal–Wallis test yielded H = 8.833, p = 0.065, which was slightly above the 0.05 significance threshold. This discrepancy indicates that the inferential conclusion is sensitive to the analytical method used for these small samples. Although the prespecified parametric ANOVA indicated statistically significant between-group differences, the nonsignificant rank-based result should be retained as an indication of uncertainty rather than dismissed solely on the grounds of statistical power.

Tukey HSD Advanced Test

Table 5
Comparison of Tukey HSD pairs

Spouse (wt.%)	Average difference G1-G2	95% CI	p corrected	Verdict
0 vs 1	9,027	1,817 to 16,236	0,014	Significant
0 vs 3	2,830	-4,380 to 10,040	0,702	Insignificant
0 vs 5	3,560	-3,650 to 10,770	0,515	Insignificant
0 vs 7	0,957	-6,253 to 8,166	0,991	Insignificant
1 vs 3	-6,197	-13,406 to 1,013	0,102	Insignificant
1 vs 5	-5,467	-12,676 to 1,743	0,168	Insignificant
1 vs 7	-8,070	-15,280 to -0.860	0,027	Significant
3 vs 5	0,730	-6,480 to 7,940	0,997	Insignificant
3 vs 7	-1,873	-9,083 to 5,336	0,907	Insignificant
5 vs 7	-2,603	-9,813 to 4,606	0,758	Insignificant

Note: a positive difference means that the average of the first group is higher than the second group.

Tukey's HSD test showed that the control (0 wt.% TiO_2) had a significantly higher mean flexural strength than the 1 wt.% group, with a difference of 9.027 MPa. Similarly, the 7 wt.% group had a significantly higher mean than the 1 wt.% group, with a difference of 8.070 MPa. The remaining pairwise comparisons were not statistically significant at $\alpha = 0.05$. The letter-group representation classified the 0 and 7 wt.% groups as group a, the 1 wt.% group as group b, and the 3 and 5 wt.% groups as intermediate groups ab. These results indicate that the most pronounced reduction occurred at 1 wt.% TiO_2, rather than demonstrating a strength increase above the control at higher contents. The pairwise comparisons should be interpreted at the specimen level and in conjunction with the small sample size and replication limitations described above.

Fault Surface Morphology

Figures 5 and 6 show the fracture-surface morphology at each TiO_2 content level. At 100× magnification, the observed fields showed rounded-to-oval cross-sections of coconut fiber bundles approximately 230–300 μm in diameter protruding from the matrix fracture plane. The fiber cross-sections appeared porous because they consisted of multiple lumen-containing ultimate fiber cells. Protruding fiber ends, empty fiber sockets, and gaps around the fibers indicate that the observed fracture involved interfacial debonding and fiber pull-out, rather than exclusively brittle fracture of the matrix. These features were identified in representative fields of view and should not be generalized to all specimens within a formulation.

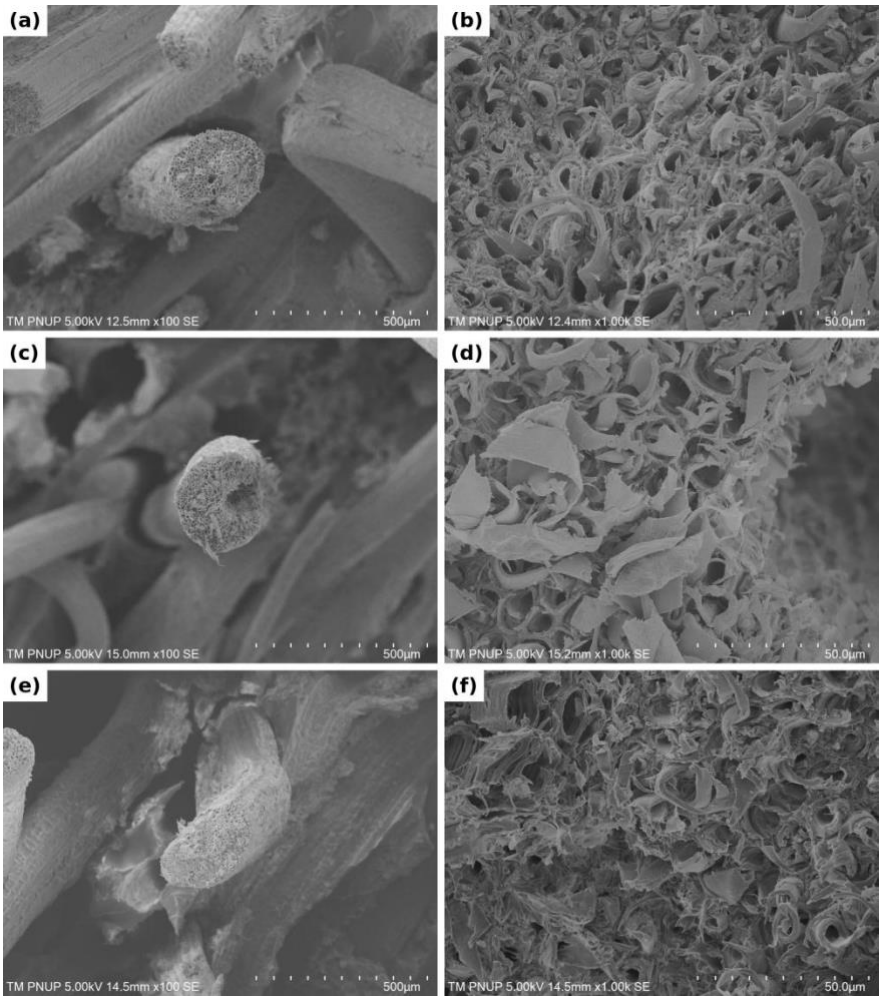


Figure 5. SEM fracture-surface morphology at (a–b) 0 wt.%, (c–d) 1 wt.%, and (e–f) 3 wt.% TiO_2; left column 100× and right column 1,000× (SE mode, 5 kV).

In the 0 wt.% control (Figure 5a), some fibers protruded considerably from the matrix, exhibiting relatively smooth lateral surfaces with partial resin coverage and gaps between the fibers and the surrounding matrix. This pattern is consistent with limited fiber–matrix adhesion in the untreated fibers. At 1 wt.% (Figure 5c), the protruding fibers appeared insufficiently bonded to the surrounding matrix, and dark regions were visible in the background outside the focal plane. At 3 wt.% (Figure 5e), interfacial gaps were clearly visible along the curved lateral surfaces of the fibers, providing qualitative evidence of local debonding. In contrast, at 5 wt.% (Figure 6a) and 7 wt.% (Figure 6c), the fiber bundles generally appeared fractured closer to the matrix plane, while the surrounding epoxy matrix exhibited radial lines, or river and hackle marks, consistent with brittle crack propagation. Both formulations also exhibited spherical cavities ranging from tens of micrometers to approximately 130 µm, as well as fiber sockets containing displaced or missing fibers. These observations indicate that potential processing defects remained visible at higher TiO_2 contents.

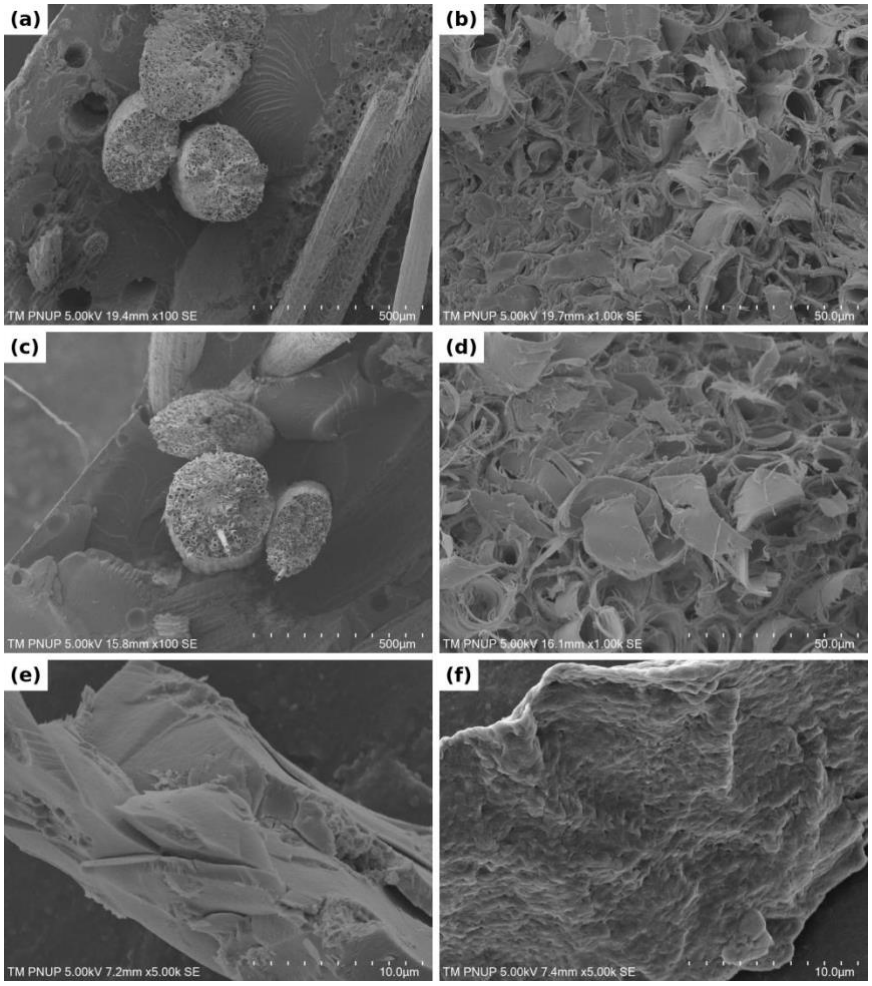


Figure 6. SEM fracture-surface morphology at (a–b) 5 wt.% and (c–d) 7 wt.% TiO_2 at 100× and 1,000×, with (e–f) representative 7 wt.% surface details at 5,000× (SE mode, 5 kV).

Discussion

At 1,000× magnification (Figures 5b, 5d, 5f, 6b, and 6d), the fiber cross-sections at all TiO_2 content levels exhibited a honeycomb-like cellular arrangement, with cell diameters of approximately 8–12 µm. The cell walls appeared torn, rolled, and fibrillated, while some lumens appeared collapsed. This morphology suggests that some fibers fractured and that their cell walls underwent separation and opening along the microfibrillar structure, rather than being pulled out entirely intact. No systematic differences in the internal fiber structure were apparent among the tested content levels. This observation is consistent with the use of untreated fibers and the incorporation of TiO_2 into the resin rather than directly into the fibers. Accordingly, the differences in flexural strength may be more closely associated with interfacial conditions, matrix defects, and fiber distribution than with changes in the intrinsic internal structure of the fibers.

At 5,000× magnification, the 7 wt.% specimen (Figures 6e and 6f) exhibited layered fracture features with irregular edges, microcracks, and clusters of fine particles in some locations, while other regions displayed coarse, undulating textures. However, SE images without energy-dispersive X-ray spectroscopy (EDS) cannot reliably distinguish TiO_2 particles from matrix or fiber fragments based on morphology alone. Furthermore, the 1,000× images were acquired at fiber cross-sections rather than specifically within the matrix. Therefore, the presence, distribution, and agglomeration of TiO_2 within the matrix could not be directly established from the available images.

Qualitatively, the interfacial gaps observed in the 1 and 3 wt.% formulations were consistent with their lower mean flexural strengths relative to the control, while the flatter fiber fractures closer to the matrix plane observed in the representative 5 and 7 wt.% images coincided with numerical strength recovery. This correspondence remains indicative rather than conclusive because each content level was represented by a single field of view, fiber pull-out was also observed in the control, and voids remained visible at higher TiO_2 contents. Quantitative

measurements of fiber pull-out length, void fraction, and titanium distribution using backscattered-electron (BSE) imaging and EDS would be required to evaluate these proposed relationships more rigorously.

Interpretation of the Mechanism

The sharp decrease in flexural strength observed at 1 wt.% may be associated with changes in resin rheology, local wetting, particle distribution, or defect formation. However, TiO_2 dispersion, resin viscosity, particle agglomeration, and defect density were not measured directly. Consequently, the SEM images cannot establish that TiO_2 itself caused the reduction in strength. The observed interfacial gaps and fiber pull-out are treated as qualitative evidence of local fracture behavior, whereas the proposed explanations involving rheology and crack-path changes remain hypotheses for future investigation.

The numerical recovery in mean flexural strength observed at 3–7 wt.% may be associated with changes in matrix constraint, crack-path deflection, or particle-mediated space filling, but these mechanisms were not quantified directly. At 7 wt.%, two specimens exceeded the control mean, whereas one specimen exhibited substantially lower strength, indicating pronounced specimen-level variability. This pattern is also consistent with potential heterogeneity in particle dispersion, fiber distribution, or void content. Without EDS mapping, rheological measurements, and quantitative defect characterization, a causal mechanism attributable to TiO_2 cannot be confirmed.

Comparison with Literature

Unlike Krishna et al. (2025) and Prabhu et al. (2024) who reported the best bending or flexural properties at 2 wt.% TiO_2, the present study exhibited a minimum at 1 wt.% followed by numerical recovery at higher contents. These differences may reflect variations in fiber type and treatment, TiO_2 particle size and phase, epoxy formulation, fiber fraction, the mass basis used to calculate wt.%, dispersion procedures, and curing history. The bamboo and luffa systems examined in the previous studies do not provide a direct basis for absolute-value comparisons with untreated, randomly distributed coconut coir fibers. Nevertheless, those studies help demonstrate that the flexural response to TiO_2 is material-specific. Accordingly, the novelty of the present study lies in the formulation-specific response observed in the coconut coir–epoxy dataset, together with an explicit analysis of uncertainty, rather than in assuming that an optimum reported for another natural-fiber system is directly transferable. Several relevant parameters differ between the studies or are not fully documented for the present dataset; therefore, the comparison supports a material-specific interpretation rather than the identification of a universally applicable optimum.

The control exhibited the highest mean flexural strength, demonstrating that filler addition did not necessarily improve the measured mechanical response. TiO_2 may be beneficial when improvements in stiffness, load transfer, or resistance to crack propagation outweigh potential losses associated with particle agglomeration, void formation, or impaired wetting. These considerations are consistent with the principle that particle dispersion and interfacial quality can be as important as filler content (Prasad et al., 2018; Wang et al., 2015).

Limitations and Implications

The principal limitations of this study include three replicates per content level, an unclear basis for the independence of the replication panel, and the unavailability of specimen dimensions, support span lengths, test rates, load–deflection curves, and documented failure modes. SEM characterization was qualitative and limited to one field of view per content level, without EDS analysis. Agglomerate size, density, and void fraction were also not quantified. Consequently, the results may indicate formulation-related differences within the tested specimen set, but they are insufficient to establish an optimal formulation or a definitive processing mechanism. These limitations constrain reproducibility, external validity, and process-level causal interpretation. All conclusions should therefore remain restricted to the tested specimens and the documented experimental conditions.

Within the tested specimen set, the 1 wt.% formulation exhibited a statistically

significantly lower mean flexural strength than both the control and 7 wt.% groups. This result warrants further investigation but does not justify a general recommendation to avoid that formulation under all conditions. The 7 wt.% formulation, whose mean strength approached the control mean but exhibited relatively high variability, should be regarded as a candidate for further investigation rather than an established optimum. Confirmatory studies should use independent manufacturing panels, larger sample sizes, complete ASTM D790-25 test documentation, controlled dispersion and curing records, quantitative void analysis, and SEM/EDS-based characterization before practical formulation recommendations are made.

CONCLUSION

Across the tested formulations, mean flexural strength exhibited a nonlinear pattern: 31.61 ± 3.75 MPa at 0 wt.%, 22.59 ± 0.62 MPa at 1 wt.%, 28.78 ± 1.42 MPa at 3 wt.%, 28.05 ± 0.87 MPa at 5 wt.%, and 30.66 ± 4.34 MPa at 7 wt.% TiO_2. One-way ANOVA indicated statistically significant between-group differences, $F(4, 10) = 5.153$, $p = 0.016$, with $\eta^2 = 0.673$ and $\omega^2 = 0.526$. Tukey's HSD test identified statistically significant differences between the 0 and 1 wt.% groups and between the 1 and 7 wt.% groups. No TiO_2-filled formulation demonstrated a statistically significant improvement over the control. Representative SEM images revealed interfacial debonding, fiber pull-out, fibrillation, interfacial gaps, microcracks, and voids. However, these observations are qualitative and do not establish the causal mechanisms underlying the observed strength differences.

Given the sample size of three specimens per formulation, unresolved uncertainty regarding manufacturing-panel independence, incomplete ASTM D790-25 test metadata, and the absence of quantitative void measurements and EDS data, the findings are restricted to the tested specimen set. The 7 wt.% formulation showed the closest numerical recovery toward the control mean among the filled groups but should be considered a candidate for further investigation rather than an established optimum. Similarly, the lower mean strength observed at 1 wt.% does not justify a general recommendation beyond the tested conditions. Independent manufacturing-panel replication, larger sample sizes, complete load–deflection and specimen-dimension records, and quantitative microstructural characterization are required before formulation recommendations or mechanistic claims can be generalized.

ACKNOWLEDGEMENT

The author would like to thank the Politeknik Ilmu Pelayaran Makassar and the Politeknik Negeri Ujung Pandang for the institutional support and the provision of laboratory facilities used in the manufacture of composite panels, three-point loading testing, and observation of fault surface morphology using SEM in this study.

AUTHOR CONTRIBUTION STATEMENT

Mahadir Sirman: conceptualization, methodology, specimen making, statistical data analysis, and writing of the initial draft of the manuscript. Syahrizal: investigation, specimen testing and SEM characterization, as well as data validation. Muhammad Arsyad Suyuti: supervision, provision of testing resources, and writing – review and editing of the final manuscript. All authors have read and approved the published manuscript.

REFERENCES

Anbanandam, K., Yadav, S. K., Ponnuswamy, R., Durairaj, W. J. V. S., Dhakshnamurthy, V. K., & Ramasamy, G. (2026). Improved mechanical and tribological behaviour of peepal–okra–madar fiber hybrid composites reinforced with TiO 2 nanoparticles . *EPJ Web of Conferences*, *370*. https://doi.org/10.1051/epjconf/202637001002

ASTM International. (2025). ASTM D790-25: Standard test methods for flexural properties of unreinforced and reinforced plastics and electrical insulating materials. ASTM International. https://doi.org/10.1520/D0790-25

Balaji, D., Kumar, P. S., Bhuvaneshwari, V., Rajeshkumar, L., Singh, M. K., Sanjay, M. R., & Siengchin, S. (2025). A review on effect of nanoparticle addition on thermal behavior of natural fiber–reinforced composites. In *Heliyon* (Vol. 11, Number 1). https://doi.org/10.1016/j.heliyon.2024.e41192

Brailson Mansingh, B., Binoj, J. S., Siengchin, S., & Sanjay, M. R. (2023). Influence of surface treatment on properties of *Cocos nucifera L. Var typica* fiber reinforced polymer composites. *Journal of Applied Polymer Science*, *140*(3). https://doi.org/10.1002/app.53345

Deeban, B., Komali, K., Illango, E., & Sarathi, A. (2026). Mechanical, moisture absorption, and morphological analysis of epoxy composites reinforced with natural fibres. *Iranian Polymer Journal (English Edition)*, *35*(3). https://doi.org/10.1007/s13726-025-01580-1

Faria, D. L., Júnior, L. M., Resende, A. A., Lopes, D. E., Mendes, L. M., Martins, M. A., Marconcini, J. M., & Junior, J. B. G. (2020). Physical and mechanical properties of polyurethane thermoset matrices reinforced with green coconut fibres. *Journal of Composite Materials*, *54*(30), 4841–4852. https://doi.org/10.1177/0021998320940023

Foruzanmehr, Mr., Vuillaume, P. Y., Robert, M., & Elkoun, S. (2015). The effect of grafting a nano-TiO2 thin film on physical and mechanical properties of cellulosic natural fibers. *Materials and Design*, *85*. https://doi.org/10.1016/j.matdes.2015.06.105

Kallel, M., & Elleuch, K. (2025). Review on three-point bending test for evaluating the mechanical properties, fracture behavior, and adhesion strength of coating/substrate systems. In *Materialpruefung/Materials Testing* (Vol. 67, Number 5). https://doi.org/10.1515/mt-2024-0447

Kamarudin, S. H., Mohd Basri, M. S., Rayung, M., Abu, F., Ahmad, S., Norizan, M. N., Osman, S., Sarifuddin, N., Desa, M. S. Z. M., Abdullah, U. H., Mohamed Amin Tawakkal, I. S., & Abdullah, L. C. (2022). A Review on Natural Fiber Reinforced Polymer Composites (NFRPC) for Sustainable Industrial Applications. In *Polymers* (Vol. 14, Number 17). https://doi.org/10.3390/polym14173698

Khokhlov, A. V., Galyshev, S. N., Atanov, B. I., & Orlov, V. I. (2025). Effect of Delamination of Low Shear Strength Materials on Fracture and Test Results under Three-Point Bending. *Physical Mesomechanics*, *28*(4). https://doi.org/10.1134/S102995992460157X

Krishna, M. G., NagarajaGanesh, B., Rekha, B., & Ganeshan, P. (2025). Nano-TiO2 grafted Luffa cylindrica fibers and their effect on the mechanical and water repellent properties of epoxy composites. *Next Materials*, *9*, 101269. https://doi.org/10.1016/j.nxmate.2025.101269

Madueke, C. I., Ekechukwu, O. M., & Kolawole, F. O. (2024). A Review on Coir Fibre, Coir Fibre Reinforced Polymer Composites and Their Current Applications. In *Journal of Renewable Materials* (Vol. 12, Number 12). https://doi.org/10.32604/jrm.2024.055207

Nissar, M., N, C. K., Birjerane, Y. A., Patil, S., Shetty, S., & Das, A. (2025). Coconut Coir Fiber Composites for Sustainable Architecture: A Comprehensive Review of Properties, Processing, and Applications. In *Journal of Composites Science* (Vol. 9, Number 10). https://doi.org/10.3390/jcs9100516

Okpala, C. C., Chinwuko, E. C., & Daniel, E. C. (2021). Mechanical Properties and Applications of Coir Fiber Reinforced Composites. *SSRN Electronic Journal*. https://doi.org/10.2139/ssrn.3877176

Prabhu, R., Mendonca, S., Bellairu, P. K., DSouza, R. C., & Bhat, T. (2024). Effect of TiO_2 filler on mechanical and tribological properties of Owen bamboo fiber reinforced epoxy composite. *World Journal of Engineering*, *21*(4), 781–792. https://doi.org/10.1108/WJE-12-2022-0495

Prasad, V., Joseph, M. A., & Sekar, K. (2018). Investigation of mechanical, thermal and water absorption properties of flax fibre reinforced epoxy composite with nano TiO2 addition. *Composites Part A: Applied Science and Manufacturing*, *115*, 360–370. https://doi.org/10.1016/j.compositesa.2018.09.031

Sankaran, S., Palani, G., Yang, Y. L., & Trilaksana, H. (2025). Enhancing natural fiber-based polymeric composites with biochar filler particles derived from groundnut shell biomass waste. *Biomass Conversion and Biorefinery*, *15*(9). https://doi.org/10.1007/s13399-024-06201-0

Skosana, S. J., Khoathane, C., & Malwela, T. (2025). Driving towards sustainability: A review of natural fiber reinforced polymer composites for eco-friendly automotive light-weighting. In *Journal of Thermoplastic Composite Materials* (Vol. 38, Number 2). https://doi.org/10.1177/08927057241254324

Song, W., Fan, W., Liu, T., Chen, X., Wang, S., Zhao, Y., Song, C., Mi, P., Dou, H., & Gao, X. (2021). Flexural fatigue properties and failure propagation of 3D stitched composites under 3-point bending loading. *International Journal of Fatigue*, *153*. https://doi.org/10.1016/j.ijfatigue.2021.106507

Wang, H., Xian, G., & Li, H. (2015). Grafting of nano-TiO2 onto flax fibers and the enhancement of the mechanical properties of the flax fiber and flax fiber/epoxy composite. *Composites Part A: Applied Science and Manufacturing*, *76*, 172–180. https://doi.org/10.1016/j.compositesa.2015.05.027